POLITECNICO DI TORINO
Repository ISTITUZIONALE

Plasmon-enhanced light absorption in mid-wavelength infrared HgCdTe detectors

(Article begins on next page)

27 April 2024

Plasmon-Enhanced Light Absorption in Mid-Wavelength Infrared HgCdTe Detectors

Marco Vallone, Alberto Tibaldi, *Member, IEEE*, Stefan Hanna, Anne Wegmann, Detlef Eich, Heinrich Figgemeier, Francesco Bertazzi, Giovanni Ghione, *Fellow, IEEE,* and Michele Goano, *Senior Member, IEEE*

Abstract—**Multiphysics modeling of a planar HgCdTe-based mid-wavelength infrared (MWIR) focal plane array with $3\,\mu$m-wide pixels enlightens the role of surface plasmon-polaritons observed in gold nanorods arranged on its illuminated face. Simulations indicate that the proposed plasmonic detector, which employs a $1\,\mu$m-thick absorber layer, exhibits a reduction of diffusive inter-pixel crosstalk by more than one order of magnitude with respect to more conventional, non-plasmonic detectors with a $5\,\mu$m-thick absorber layer, without penalizing responsivity and achieving increased detectivity in the whole MWIR band by taking advantage of the absorber volume reduction.**

Index Terms—**Infrared detectors, plasmonics, HgCdTe, focal plane arrays, FDTD.**

I. INTRODUCTION

SURFACE plasmon polaritons (SPP) are the quasiparticles associated with plasma oscillations of free electrons coupled with electromagnetic fields, and localized along dielectric–metal interfaces [1]. Illuminating a plasmonic nanostructure, e.g. gold (Au), silver (Ag) or aluminum (Al) nanospheres, nanorods, or differently shaped particles, arranged on the illuminated face of a photodetector, collective oscillations of free electrons can be excited [2], [3]. At wavelengths determined by the nanostructure characteristics, the illuminating radiation may strongly interact and couple with these oscillations, resulting in a significant enhancement of the electromagnetic wave's electric field around the plasmonic nanostructures and increasing the light absorption efficiency. Several solutions have been experimentally characterized and simulated, demonstrating SPP-induced absorption enhancement in terahertz [4] and in infrared (IR) detectors operating in the MWIR (mid-wavelength IR, $\lambda \in [3, 5]\,\mu$m) and LWIR (long-wavelength IR, $\lambda \in [8, 12]\,\mu$m) bands. With regard to the IR detectors, metallic (Au, Ag, etc.) or transparent conducting oxide (TCO) nanoelements, e.g., Sn-doped In oxide (Indium-Tin Oxide, ITO) nanorods, have been considered, showing that their performance strongly depends on their size, shape, and doping concentration [5], [6], [7], [8], [9], [10], [11], [12]. Metal–semiconductor–metal (MSM) schemes [13]

with variously shaped nanoelements have been explored to reduce the noise equivalent temperature difference (NETD, see the definition in [14, Sec. 19.4]), and the noise associated with high operating temperature (HOT) detectors [15], [16]. HOT detectors are heterostructures with combinations of exclusion and extraction junctions. They operate in reverse bias and allow to suppress Auger generation by reducing the carrier density in the absorber layer below thermal equilibrium [17], [18]. A MSM scheme designed for a not-absorbing cavity [19] demonstrated the tunability of the resonances in the MWIR and LWIR bands. In solar cells, significant plasmonic field enhancement induced by self-assembled metallic nanoparticles randomly dispersed on the detector illuminated face has been demonstrated [20], [21], [22]. Notable experimental works concern plasmonic absorption enhancement in InAs/GaAs quantum-dot [23], [24] and AlGaAs/GaAs quantum-well [25] infrared detectors in the LWIR band, where the absorption enhancement is provided by a metallic photonic crystal. Metal (Au)-Ge-type II strained superlattices resonators, employed as photodetectors in the MWIR band, demonstrated a maximum spectral enhancement factor of 2.5 around $\lambda = 3.8\,\mu$m [26]. Ref. [27] addresses the electromagnetic modeling and experimental characterization of quantum-well infrared detectors with gold-based two-dimensional grating resonators with several possible shapes, both for MWIR and LWIR, with single-band and dual-band architecture. In Ref. [28], a two-dimensional metal plasmonic grating is employed to enhance the quantum efficiency of nBn infrared barrier detectors [29] with absorbers as thin as $0.5\,\mu$m. Ref. [30] presents metal-insulator-metal infrared plasmonic metamaterial absorber, consisting of deep subwavelength meander line nanoantennas, resonating in the LWIR band. However, the majority of modeling contributions in the literature do not include three-dimensional, multiphysics (e.g., full-wave electromagnetic, followed by electrical transport) simulations, except for very recent examples (see, e.g., Ref. [31]).

The focus of the present work is placed on focal plane arrays (FPAs). They are extensively employed in high quality IR cameras for scientific, civilian and defense purposes [32], [33]. In FPAs, each pixel acts as a single photodetector, which can be designed as a reverse biased photodiode, possibly including complex heterostructures [34], [35]. HgCdTe (often referred to as MCT) is one of the most widely adopted compounds in this kind of devices [32], [36], [33], but the difficulty to fabricate large format IR-FPAs with small pixel pitch, low dark current [37], [38], high detectivity [14, Sec. 2.4], high responsivity and low NETD is still a major issue. The responsivity $\mathcal{R}$

M. Vallone, A. Tibaldi, F. Bertazzi, G. Ghione, and M. Goano are with the Dipartimento di Elettronica e Telecomunicazioni, Politecnico di Torino, Corso Duca degli Abruzzi 24, 10129, Torino (TO), Italia. e-mail: alberto.tibaldi@polito.it

A. Tibaldi, F. Bertazzi, and M. Goano are also with the Istituto di Elettronica e di Ingegneria dell'Informazione e delle Telecomunicazioni, Consiglio Nazionale delle Ricerche c/o Politecnico di Torino.

S. Hanna, A. Wegmann, D. Eich, and H. Figgemeier are with AIM Infrarot-Module GmbH, Theresienstraße 2, D-74072 Heilbronn, Germany.

(defined as the ratio of the photocurrent to the input optical power) can be enhanced by carefully designed multi-layer anti-reflection coatings (ARCs) [39]. However, in a number of special applications, an ARC may not be the best solution. Airborne infrared photodetectors designed for defense and civilian applications and IR cameras for atmospheric monitoring or for advanced infrared astronomy are currently moving towards the adoption of large-format 3rd-generation FPAs operating in the MWIR and LWIR bands at the same time (multi-color and multi-band IR detectors) [40]. The multi-band operation, and the request to operate with different (also wide) angle of incidence, can make the classical, multi-layer ARCs ineffective [41]. Moreover, in case of IR photodetectors employed in space missions, the mismatch between the thermal expansion coefficients of ARC and active region may be a concern, because of the thermal cycling to which robotic spacecrafts employed in Solar System explorations are exposed [42], [43].

New generation, anti-reflective solutions for such applications include engineered surfaces, like arrays of pyramidal, sinusoidal or web-like anti-reflective textures [42], light-trapping nanostructures [32], [44], [45], zero-contrast sub-wavelength gratings [46], [47], where nanoelements are fabricated directly on the surface of the absorbing material. In this context, the adoption of nanopatterned surfaces exploiting SPP resonances can be a valid alternative to ARCs. Firstly, plasmonic nanopatterned surfaces, obtained, e.g., by the deposition of Au nanostructures directly on the absorber's illuminated face, may constitute an efficient light-trapping structure. They may favor light absorption, avoiding and substituting the classical multilayer ARC solution whenever the operating environment, the bandwidth requirement, or the illumination conditions can represent a concern. Secondly, SPPs may significantly enhance the electromagnetic wave's electric field around them [11], [48], and the two mechanisms together may lead to a significant increase of $\mathcal{R}$ for wavelengths determined by the nanorods distribution itself and by the characteristics of adopted plasmonic material.

In the present contribution, the choice of vertical nanorods with circularly-symmetric shape as shown in Fig. 1 and described in detail in Section II should alleviate polarization dependence: in fact, circular shapes (nanorods, nanospheres, etc.) are polarization independent for normal incidence because of their rotational invariance (the only rotational non-invariant part of the detector is the pixel itself, which normally has a square symmetry). Nevertheless, by changing the incidence angle, the light polarization should matter, and this point will be described in a separate contribution.

Another straighforward way to enhance $\mathcal{R}$ is to increase the absorber thickness t_abs. However, for larger t_abs, the thermal generation-recombination (G-R) noise and the transit time of photogenerated carriers increase. Therefore, generally this cannot be a viable solution. Indeed, the thermal G-R rate enters in the expression of one of the most important figures of merit, the normalized detectivity D^* [14, Sec. 2.4]. The photodetector performance can be enhanced by maximixing D^*, which is defined as

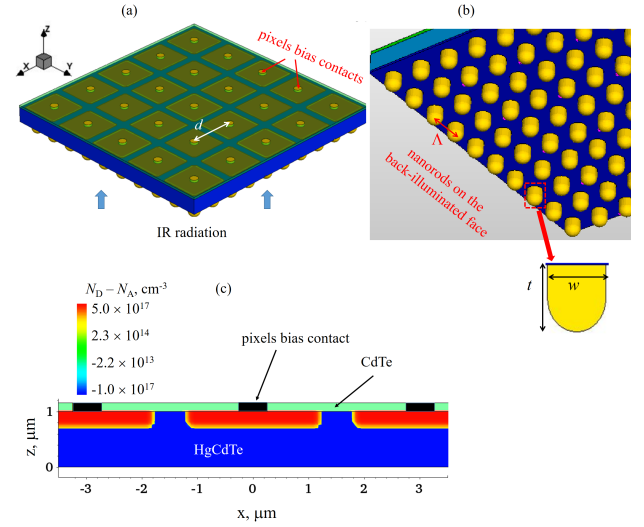$$D^* = \frac{\mathcal{R}}{q\sqrt{2G_\text{th}t_\text{abs}}}, \tag{1}$$

Fig. 1. (a) 3D MWIR 5×5 miniarray with (b) nanorods on the illuminated face, representative of a large format FPA. The pixel pitch is d, and the nanorods are Λ-spaced. (c) Vertical two-dimensional cutplane along the miniarray center, showing the doping profile.

where q is the elementary charge. Maximizing D^* requires increasing the responsivity and reducing t_abs and the carrier thermal generation rate per unit volume G_th (here considered uniform). Device cooling is an obvious remedy to reduce G_th, but cost and weight constraints on the final product suggest to move in the opposite direction, i.e., towards the development of HOT detectors [40] which include, e.g., unipolar barrier detectors and fully depleted heterostructures [49], [50]. However, the former require non-trivial composition or doping profiles, while the latter often need high reverse bias to curtail the dark current.

Eq. (1) suggests an alternative solution: SPPs, excited e.g. by a periodic array of metallic nanorods on the detector illuminated face, may allow for reducing t_abs without decreasing $\mathcal{R}$, resulting in a larger detectivity D^* and in a more HOT-behaving detector. In this context, the present contribution is focused on three-dimensional (3D) multiphysics (electromagnetic and electrical transport) modeling of a planar, HgCdTe-based, diffraction-limited [51] MWIR FPA detector, which indicate the possibility to reduce the FPA absorber thickness to $1\,\mu$m only: it can be remarked that the conventional choice for t_abs ranges between 3 and $5\,\mu$m, in the order of the average absorption length in the MWIR band [14, Sec. 3.2.3], [45]. Indeed, in the present contribution, simulations show that the adoption of FPAs with plasmonic nanostructured illuminated face significantly enhances the responsivity, making thin detectors ($t_\text{abs} = 1\,\mu$m) competitive with conventional thicker detectors without plasmonic surfaces ($t_\text{abs} = 5\,\mu$m). Correspondingly, for thin detectors, D^* is shown to be significantly increased in the whole MWIR band. Moreover, simulations at center of the MWIR band ($\lambda = 4.0\,\mu$m) indicate that the diffusive inter-pixel crosstalk [52], [53], [54] gets much decreased – more than one order of magnitude – when compared to non-plasmonic, $5\,\mu$m-thick ones. This result enables to fully exploit the imaging performance provided by

very small pixels, which may be sensitive to diffusive inter-pixel crosstalk if their thickness is larger than their pitch.

In Section II, introductory concepts at the basis of the proposed approach are provided; in Section III we describe the detector and the investigation methods; finally, in Section IV the results of multiphysics simulations and their implications are discussed, providing a motivation for the outlook on future work briefly given by Section V.

II. PLASMONICS IN IR DETECTORS

Let us consider an infinitely extended Au-MCT interface, illuminated by an electromagnetic monochromatic plane wave with wavevector $\mathbf{k}$ parallel to z, polarization vector along x (i.e., a TE mode), and λ in the MWIR band, whereas the MCT has a composition suitable to absorb light in the same band. Starting from the Maxwell equations for electric $\mathbf{E}$ and magnetic $\mathbf{H}$ fields and assuming solutions in the time-harmonic form $\mathbf{E} = E_0 \exp(\mathbf{kr} - \omega t)$ and $\mathbf{H} = H_0 \exp(\mathbf{kr} - \omega t)$, where $\omega = 2\pi c/\lambda$ is the angular frequency and c is the light velocity in vacuum, it is possible to demonstrate [1] that along the interface a TM mode exists. The wavevector components along x and z are:

$$k_x = \frac{\omega}{c}\sqrt{\frac{\epsilon_{Au}\epsilon_{MCT}}{\epsilon_{Au} + \epsilon_{MCT}}}, \quad k_z = \frac{\omega}{c}\sqrt{\frac{\epsilon_{Au}^2}{\epsilon_{Au} + \epsilon_{MCT}}}, \quad (2)$$

where ϵ_{Au} and ϵ_{MCT} are the frequency-dependent gold and MCT dielectric functions, respectively. For MCT we adopted the wavelength, temperature, and composition dependent form in [55], and for ϵ_{Au} the Drude form in Ref. [56],

$$\epsilon_{Au} = \epsilon_\infty - \frac{\omega_p^2}{\omega^2 - i\omega\omega_t}, \quad (3)$$

where $\epsilon_\infty = 1$, $\omega_p = 1.37 \times 10^{16}$ rad/s, and $\omega_t = 4.65 \times 10^{13}$ rad/s. The mode – a SPP mode – is propagating along x and evanescent along z, because in the MWIR band k_x has a large real part (especially close to the cutoff wavelength), whereas k_z has a large imaginary part. $\mathbf{E}$ has a large component along z, and the mode penetrates into the MCT layer, getting eventually absorbed during the propagation along x.

Beyond this simple case, more interesting features involve periodic, metallic nanostructures. Let us consider now a Λ-periodic, two-dimensional (2D) array of Au nanorods on the illuminated face of a MCT-based photodetector. Analytic forms for dispersion relations similar to Eq. (2) are available only for simple, regular shapes. However, in order to understand the general behavior, we will consider at first Eq. (2), equating k_x to the nanorod array wavevectors $k_{p,q} = (p\hat{x} + q\hat{y})2\pi/\Lambda$, where p and q are integers denoting the mode orders along the x- and y-directions, being $\hat{x}$, $\hat{y}$ unit vectors in the xy-plane (see Ref. [8] and references therein). It is possible to choose Λ to have a Bragg-like resonance condition for wavelengths $\lambda_{p,q}$ in the MWIR band, where

$$\lambda_{p,q} = \frac{\Lambda}{\sqrt{p^2 + q^2}} \Re \sqrt{\frac{\epsilon_{Au}(\lambda_{p,q})\epsilon_{MCT}(\lambda_{p,q})}{\epsilon_{Au}(\lambda_{p,q}) + \epsilon_{MCT}(\lambda_{p,q})}}, \quad (4)$$

$\Re$ indicating the real part. Therefore, the Au-MCT plasmon-polariton effect gives $\mathbf{k}$ a large x-component according to

Eq. (2), and the Λ-periodicity makes the SPP to become a resonant, horizontal local mode along x, favoring strong light absorption for λ values determined by Eq. (4). In principle, an FPA with a plasmonic nanorod array (from now on, a *plasmonic* FPA) could offer a large responsivity enhancement with respect to an identical *standard* FPA without plasmonic array.

Concerning the optimal choice of FPA pixel width d, a remark is necessary: the maximum optical frequency contained in the Modulation Transfer Function (MTF) [57] of an optical system with objective diameter D and operating at wavelength λ is given by D/λ. Correspondingly, the MTF of an ideal FPA with pixel width d contains spatial frequencies up to f/d, where f is the focal length of the optics. From the Nyquist theorem, the FPA must sample the image at a spatial frequency at least twice the maximum spatial frequency contained in the optics MTF, i.e., $f/d > 2D/\lambda$, which can be written as $F\lambda/d > 2$, where $F = f/D$ is the focal ratio of the optics: this is the so-called diffraction-limited condition, and it represents the optimal choice. For the MWIR band, Ref. [51] indicates $F \approx 1.5$ with a target value for pixel pitch $d \approx 3\,\mu$m, the value we have chosen in all the simulations in the present work. Ref. [58] points out that, still remaining in the diffraction limited condition $F\lambda/d = 2$, a detector with $F = 1$ and $d = 5\,\mu$m (for example) performs exactly like a system with $F = 4$ and $d = 20\,\mu$m. Authors mean that not only the resolution is the same, but also the field-of-view, the detection range (i.e., how far a target can be identified, important in defense systems), and the signal-to-noise ratio, which depends on the $(d/F)^2$ ratio [51, Eq. (12)]. However, if the objective diameter remains the same, by reducing F by a factor of four (and the pixel size, too) the focal length is reduced by the same ratio, with an ensuing reduction of total system size, weight, and also power consumption, because of the reduced cryogenic system volume. A more complete and recent study [59] indicates as appropriate a trade-off between resolution and maximum detection range, a condition which leads to $F\lambda/d = 1.5$, i.e., somewhere in between considering the diffraction-limited ($F\lambda/d = 2$) and the detector limited operation ($F\lambda/d = 0.41$, see [51]), and an acceptable F-value of 1.2. This implies $d = 3.2\,\mu$m at center of the MWIR band, a value not far from the present work ($3\,\mu$m).

The diffraction limited condition is strictly connected to one of the most important figures of merit for FPAs, i.e., the minimum NETD that can be theoretically achieved. At sufficiently low temperature, when dark current can be neglected, it is possible to show [36] that NETD $\propto F\lambda/d$, hence, for given λ and optics, the condition $F\lambda/d = 2$ also provides the minimum achievable NETD: by reducing d further, NETD would deteriorate (i.e., it would increase), whereas wider d would not exploit the available resolution provided by the optics.

III. THE DETECTOR AND THE MODELING METHODS

Fig. 1(a,b) shows the considered detector, a 5×5 pixels miniarray, with a 2D, Λ-periodic array of w-wide and t-long Au nanorods on its illuminated face. It consists of an acceptor–doped ($N_A = 10^{15}$ cm^{-3}), t_{abs}-thick, planar $Hg_{0.714}Cd_{0.286}Te$
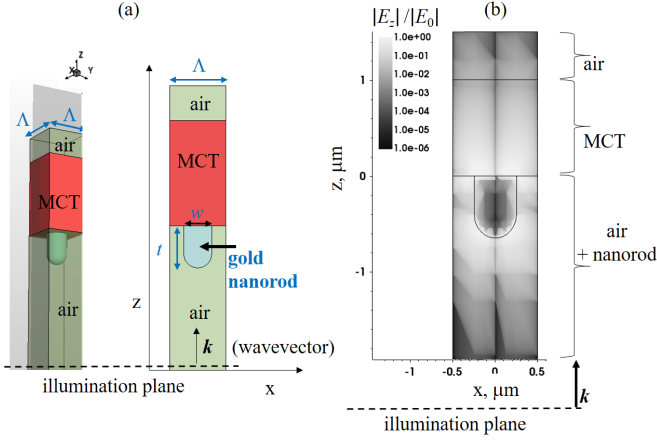
Fig. 2. (a) One of the Λ-wide square unit cells. (b) 2D cutplane of the unit cell: the z-component of the electric field in units of E_0, example for $\lambda = 4\,\mu$m, $\Lambda = 1\,\mu$m, and $w = 0.5\,\Lambda$.

layer, designed to operate at $T = 230\,$K (its cutoff wavelength is $\lambda_c \approx 4.8\,\mu$m), and all simulations in the present work have been carried out for this temperature. Pixels with a $d = 3\,\mu$m pitch are defined simulating an ion implantation on a square 2.25-micrometer-wide window with maximum donor concentration of $N_D = 5 \times 10^{17}\,$cm^{-3}, which yields a n-p junction at $\approx 0.3\,\mu$m from the bias contact (see Fig. 1(c)), and the illuminated face is located on the horizontal plane $z = 0$.

The fabrication of gold nanopillar or nanorod arrays is a known technique for solar cells [60] and biosensors [61], where gold pillar arrays were fabricated by electron beam lithography (EBL) combined with nanoscale electroplating. Gold nanopillar patterns on a ITO coated glass substrate was made using EBL [62] in organic solar cells. For the detector under study, after having grown the thin HgCdTe absorber on a standard, high quality CdTe (or CdZnTe) substrate with a standard technique (e.g. molecular beam epitaxy), the deposition of the gold plasmonic structure on the free HgCdTe face could be realized by metal evaporation and deposition, EBL and etching processes, as in [63], by standard optical EBL and metal lift-off process as in [64], or by a focused ion beam milling as in [65], whereas the bias contact could be realized through a via in the optically polished (and, if appropriate, thinned) substrate, which could become what we named passivation layer in Fig. 1. A possible way to enhance the responsivity is terminating the device with a large metallic reflector, leading to a double-pass device. This strategy is broadly used in solar cells, aiming to maximize the energy conversion. However, in this work it is not adopted, in view of avoiding capacitive effects that could deteriorate the dynamic characteristics.

As a first step, we employed the Finite Difference Time Domain (FDTD) [66], [67] electromagnetic solver Synopsys RSoft FullWAVE [68] to study a simplified problem where passivation layers and metallic contacts were neglected. The miniarray is illuminated from below with a monochromatic TE plane wave with electric field amplitude E_0, wavevector along z, and optical power flux set to $1\,$mW cm^{-2}. By imposing

periodic boundary conditions (PBCs) along x and y, and convolutional perfectly matched layer (CPML) absorbing BC along z, we could consider just one of the pixels. Moreover, by exploiting the periodicity of the structure, we subdivided the pixel into Λ-wide square unit cells, each containing one of the nanorods, as shown in Fig. 2(a). This is equivalent to simulate an infinitely extended repetition of cells, and the electromagnetic solution for one of them describes the whole FPA behavior.

Fig. 2(b) shows the distribution of the electric field component along the vertical direction E_z for one of the possible choices ($\Lambda = 1\,\mu$m, $w = 0.5\,\Lambda$, and $\lambda = 4\,\mu$m). As expected, E_z results to be quite large in the MCT absorber, especially close to the MCT-Au interface, because of the xy-stationary mode connected to the SPP.

For a given wavelength, the spatial distribution $A_{\text{opt},w}(x, y, z)$ (number of absorbed photons per unit volume and time, in a unit cell which includes a nanorod with diameter w) is obtained as the divergence of the time-averaged Poynting vector $\langle \vec{S} \rangle$ [69, Sec. 6.8] [70], [71], [72], [73], [74]

$$A_{\text{opt},w}(x, y, z) = -\frac{\vec{\nabla} \cdot \langle \vec{S}(\lambda) \rangle}{hc/\lambda}, \tag{5}$$

where the material complex refractive index is included in $\vec{S}$ e.g. as in Refs. [75], [76]. After some trial, a good SPP-induced field enhancement effect was observed for a nanorod composed by a $0.4\,\mu$m-high cylinder topped with a hemisphere, for a total thickness of $t = 0.775\,\mu$m, the presently adopted value, whereas its optimal diameter w has been chosen by means of a series of three-dimensional FDTD simulations for $\lambda = 4\,\mu$m (center of the MWIR band).

Fig. 3(a) shows the rate $A_{\text{opt},w}(x, y, z)$ integrated on the MCT volume V_{MCT} of the unit cell,

$$A(w) = \int_{V_{\text{MCT}}} A_{\text{opt},w}(x, y, z)\mathrm{d}x\,\mathrm{d}y\,\mathrm{d}z, \tag{6}$$

as function of w/Λ, for the trial value $\Lambda = 1\,\mu$m. We remark that $w = 0$ identifies a *standard* photodetector, i.e. without nanorods. It is evident that $w \approx 0.5\,\Lambda$ provides the maximum absorption in the MCT volume. Moreover, the very interesting result is that, in that case, a $1\,\mu$m thick MCT *plasmonic* absorber provides the same absorption of (or even higher than) a $2.5\,\mu$m thick *standard* absorber (point $w = 0$). Another interesting information included in Fig. 3(a) is the fact that the highest absorption enhancement due to SPPs coupling, $A(w)/A(0)$, is provided by the thinner detector, whereas it becomes less and less significant as long as t_{abs} increases.

In order to identify the optimum value for Λ, in Fig. 3(b) we show the colormap of the absorption enhancement M, defined as the ratio

$$M(\Lambda, \lambda) = \frac{A(w = 0.5\,\Lambda)}{A(w = 0)}, \tag{7}$$

as function of Λ and λ. It describes the absorption enhancement of a *plasmonic* detector with respect to the corresponding *standard* one, and the Λ value which provides first order resonance is slightly lower than $1.5\,\mu$m, and only mildly dependent on λ. It can be noticed that this value is considerably different from the value provided by Eq. (4), which represents
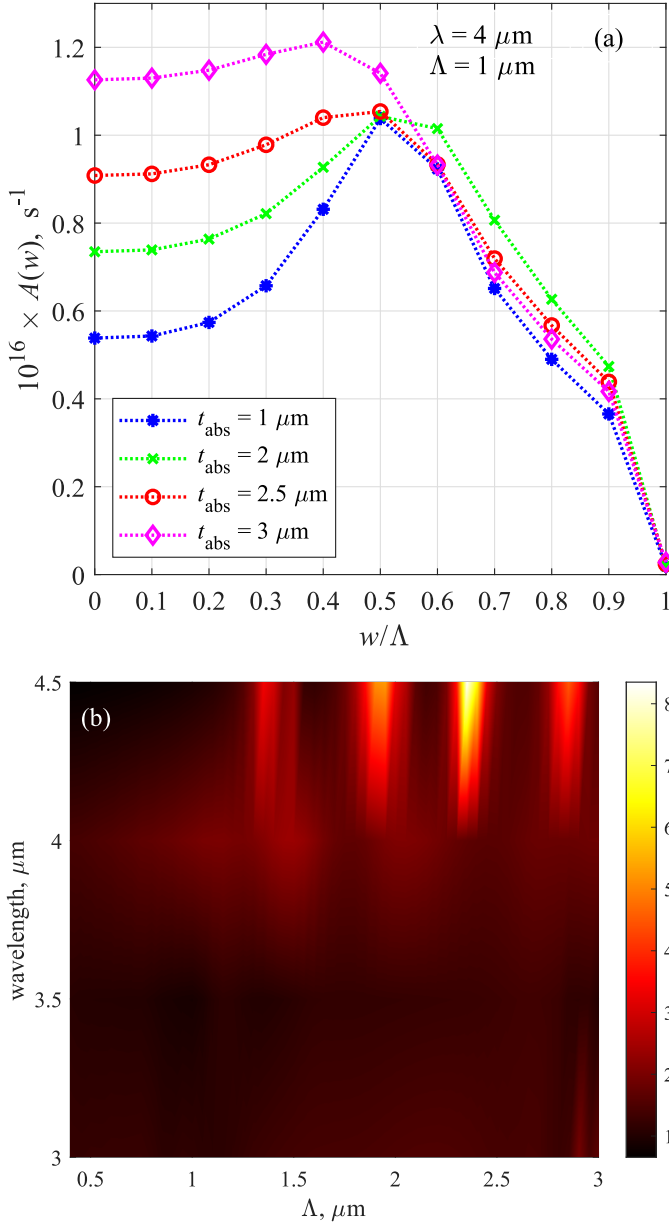
Fig. 3. (a) Absorption rate in the absorber layer of the unit cell vs. w/Λ, for $\Lambda = 1\,\mu\text{m}$, $\lambda = 4\,\mu\text{m}$ and several values of absorber thickness t_{abs}. (b) Colormap of $M(\Lambda, \lambda)$ for the unit cell and $w = 0.5\,\Lambda$.

expected performance in terms of NETD and image resolution (MTF), as discussed in Section II. Of course, for a deeper understanding of the relations between λ, d, NETD and MTF characteristics, experimental data would be useful.

IV. MULTIPHYSICS MODELING

We first considered a single pixel of the miniarray shown in Fig. 1, and the plane wave illumination condition described in Section III. Electrical transport 3D simulations have been performed in the drift-diffusion approximation following the approaches described in [54], [75], [76], [77], [78] with a commercial simulator by Synopsys [79], characterized by a highly customizable software material library. The optical generation rate distribution $G_{\text{opt},w}$ into the detector, due to interband optical absorption, has been taken equal to $A_{\text{opt},w}$ without loss of generality, and it enters as a source term in the electron and hole continuity equations. The latter have to be self-consistently solved with Poisson equation and Fermi distribution expressions, as described in detail e.g. in Ref. [76], and PBCs have been applied along x and y directions for both the electromagnetic and transport problems. $A_{\text{opt},w}$, which is defined on the optical grid (with uniform mesh size of 50 nm), has been mapped into the not uniform electrical grid, which is finer where doping gradient is higher, close to regions interfaces and electrical contacts. The dependence of HgCdTe electrical properties on composition, doping and temperature has been taken into account according to the models reported in Ref. [76] (Table I), without including possible doping-induced plasma effects in the complex refractive index, e.g., Burstein-Moss effect and free carrier absorption, [80], [81].

Electrical simulations include Auger, radiative (modeled as in Ref.[82] and in Ref. [76] (Table I)) and SRH generation-recombination processes. The latter have been modeled as in Ref. [37] considering a SRH lifetime around $100\,\mu\text{s}$, neglecting for simplicity trap-assisted [83], [84], [85] and band to band tunneling. Among the most important parameters obtained by the models in [37], we may report for ease of use the absorber's energy gap (0.2556 eV), electron mass ($0.0185\,m_0$, where m_0 is the free electron mass), hole mass ($0.55\,m_0$), radiative coefficient ($3.226 \times 10^{-11}\ \text{cm}^3\text{s}^{-1}$), electron Auger coefficient ($3.228 \times 10^{-26}\ \text{cm}^6\text{s}^{-1}$), hole Auger coefficient ($6.529 \times 10^{-27}\ \text{cm}^6\text{s}^{-1}$), electron mobility ($9507\ \text{cm}^2\text{V}^{-1}\text{s}^{-1}$), hole mobility ($95\ \text{cm}^2\text{V}^{-1}\text{s}^{-1}$), as evaluated from the cited models at $T = 230\,\text{K}$. Other important parameters depend from the illuminating wavelength (the absorption coefficient), or from the carrier density (e.g. the radiative, SRH, and Auger recombination rates) and are self-consistently evaluated during the simulation. In Fig. 4(a) the spectral responsivity $\mathcal{R}$ is shown for a *standard* and a *plasmonic* detector with $1\,\mu\text{m}$-thick absorber, and for a *standard* detector with $5\,\mu\text{m}$-thick absorber (the latter value is a common choice in MWIR FPAs [86], [45]). For the thinner absorber, the responsivity enhancement due to the plasmonic nanorods is particularly significant close to the cutoff wavelength. However, there is not a large and clear advantage coming from the adoption of $1\,\mu\text{m}$-thick *plasmonic* detector in comparison with *standard* detectors with more common absorber thickness.

an oversimplified model, able to provide a first estimate of the resonant wavelengths, but unable to account for details determined by unit cells geometry: instead, Fig. 3(b) provides an *a posteriori* better estimate of the optimal value for Λ. The third resonance, which lies at $\Lambda \approx 2.3\,\mu\text{m}$, in principle provides a much higher value for M. With the constraint to have even–spaced nanorods on the FPA, this choice would imply $d = 4.6\,\mu\text{m}$, which still represents the state-of-the-art. However, since our intention is to provide just a proof-of-concept, we set $\Lambda = 1.5\,\mu\text{m}$ and $w = 0.5\,\Lambda$, which implies $d = 3\,\mu\text{m}$. This choice represents an acceptable trade–off according to Fig. 3: it still shows the effect (even if with a reduced value for M), privileging – at least theoretically – the
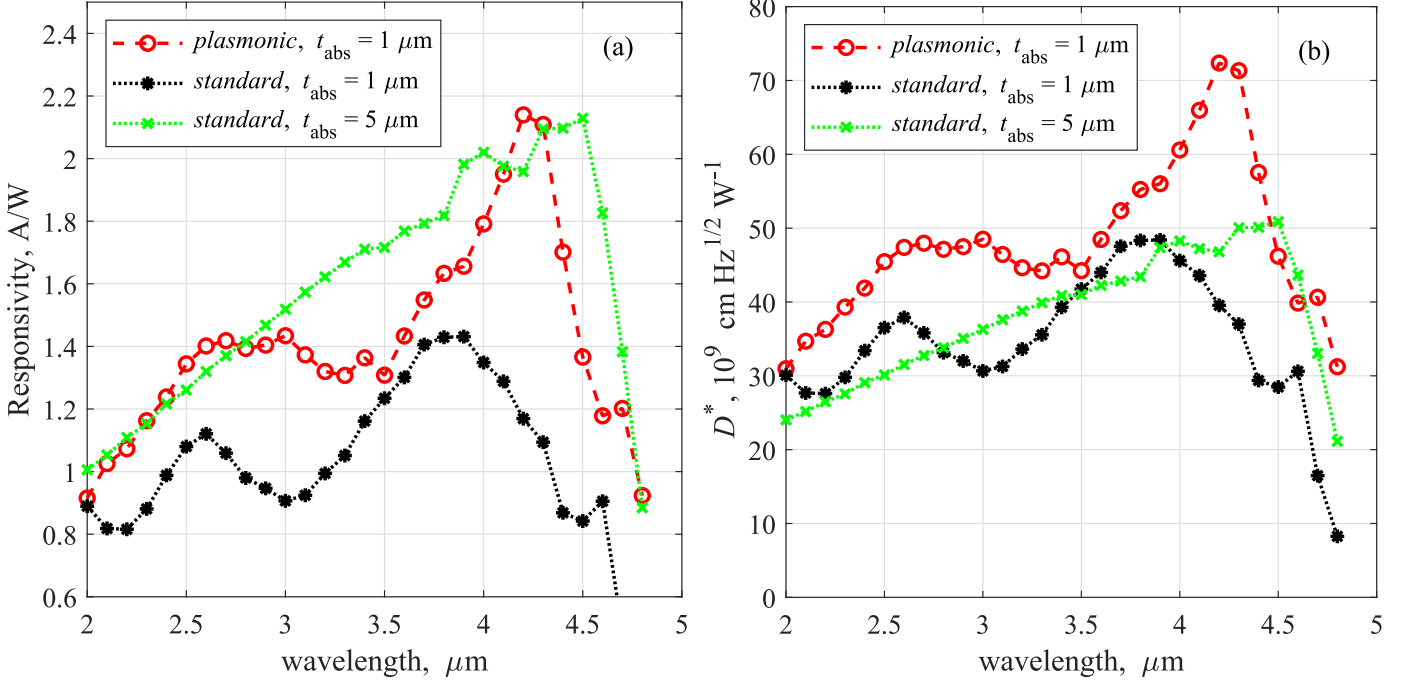
Fig. 4. Multiphysics simulations, plane wave illumination: (a) spectral responsivity $\mathcal{R}$ and (b) detectivity D^* for a *plasmonic* and a *standard* FPA with $t_{\mathrm{abs}} = 1\,\mu\mathrm{m}$ and for a *standard* FPA with $5\,\mu\mathrm{m}$.

The benefit coming from the absorber thickness reduction is more clear when considering the detectivity D^*, Eq. (1), which also contains the contribution coming from thermal generation G_{th}, and that can be redefined in a more general way as

$$D^* = \frac{\mathcal{R} S^{1/2}}{q \left(2 \int_{V_{\mathrm{MCT}}} G_{\mathrm{th}}(x,y,z) \mathrm{d}x\,\mathrm{d}y\,\mathrm{d}z \right)^{1/2}}, \qquad (8)$$

where S is the detector area. Actually, Fig. 4(b) shows a significant D^* increase for the thinner *plasmonic* detector, whose value is higher than the corresponding value for a *standard* $5\,\mu\mathrm{m}$-thick detector in the whole MWIR band. From Eq. (8), this is due to a decrease of the integral of G_{th} in the thinner detector, in association with a substantially avoided loss of responsivity thanks to the plasmonic effects (Fig. 4(a)). Moreover, other important figures of merit may benefit from a substantial reduction of the absorber thickness.

A. Possible benefits for NETD

When the operating temperature does not allow to neglect the dark current J_{dark}, NETD is worsened by an increase of J_{dark}, since in this case it is NETD $\propto \sqrt{1 + J_{\mathrm{dark}}/J_\Phi}$, where J_Φ is the total background flux current density (see [87], [36] for details). Very often J_{dark} is proportional to the absorber volume, therefore by reducing t_{abs} also NETD would be reduced. However, a simulation of NETD taking into account all the contributions strongly depends on the doping profiles, the operating temperature, and growth details, and a dedicated modeling and exerimental investigation would be appropriate, which is beyond the scope of the present work.

B. Possible benefits for inter-pixel crosstalk and response time

Let us consider now the whole 5×5 miniarray shown in Fig. 1, and indicate with CP and NNs the miniarray central pixel and its nearest neighboring pixels, respectively. When the miniarray is illuminated by a narrow, monochromatic Gaussian beam with waist radius $\approx 2.5\,\mu\mathrm{m}$, its axis along z, and centered on the CP, the illumination condition is very similar to that provided by a low F-number optical system: the beam is a wide cone, and its Fourier decomposition [88] contains components which are highly non-normal, i.e., with wide angle of incidence (a future useful investigation, not included in the present work, could directly concern the simulation of plane wave illumination with same power and variable angle of incidence). Carriers photogenerated in a given pixel tend to diffuse laterally, towards NNs, before being collected, giving origin to the diffusive inter-pixel crosstalk, which can be approximated as [53]

$$\mathcal{D}_{\mathrm{NNs}} \approx \mathcal{C}_{\mathrm{NNs}} - \mathcal{O}_{\mathrm{NNs}}, \qquad (9)$$

where the ratio between the photocurrent in the CP and in the NNs,

$$\mathcal{C}_{\mathrm{NNs}} = \frac{I_{\mathrm{ph,\,NNs}}}{I_{\mathrm{ph,\,CP}}}, \qquad (10)$$

can be regarded as a possible definition of the *total* inter-pixel crosstalk, and

$$\mathcal{O}_{\mathrm{NNs}} = \frac{\int_{V_{\mathrm{NNs}}} G_{\mathrm{opt},w}(x,y,z)\,\mathrm{d}x\,\mathrm{d}y\,\mathrm{d}z}{\int_{V_{\mathrm{CP}}} G_{\mathrm{opt},w}(x,y,z)\,\mathrm{d}x\,\mathrm{d}y\,\mathrm{d}z} \qquad (11)$$

is the optical inter-pixel crosstalk, defined as the ratio between carriers photogenerated in one of the NNs (with volume V_{NNs}) and those photogenerated in the CP (with volume V_{CP}).
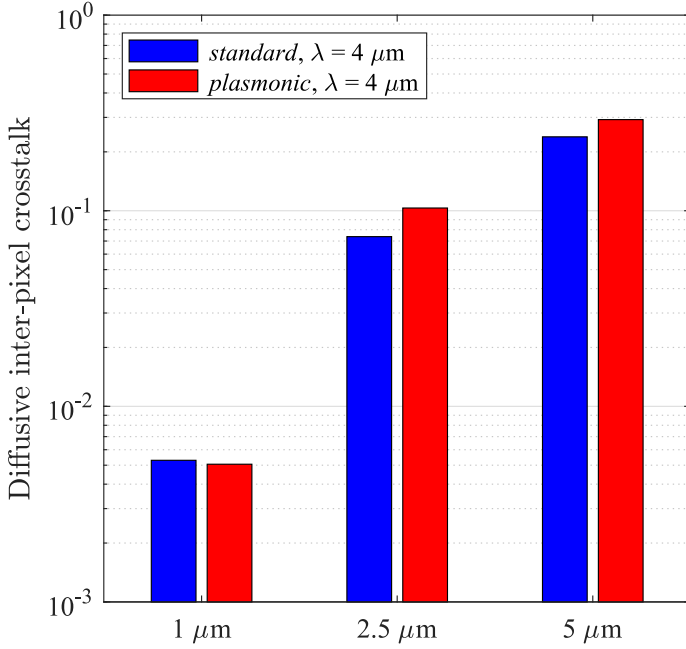
Fig. 5. Multiphysics simulations, Gaussian beam illumination at wavelength $\lambda = 4\,\mu m$: diffusive inter-pixel crosstalk $\mathcal{D}_{\mathrm{NNs}}$ for the *standard* and *plasmonic* miniarray, with $1\,\mu m$, $2.5\,\mu m$, and $5\,\mu m$-thick absorber.

Since commonly adopted values for t_{abs} in MWIR band are between $3\,\mu m$ and $5\,\mu m$ [86], [45], if d is as small as $3\,\mu m$ to fulfill both the diffraction limited condition and the minimum achievable NETD, the diffusive inter-pixel crosstalk may increase quite rapidly when t_{abs} increases. By the adoption of plasmonic nanorods, the thickness t_{abs} could be decreased safely, reducing $\mathcal{D}_{\mathrm{NNs}}$ in turn without penalizing much the responsivity (Fig. 4(a)) and increasing significantly the detectivity (Fig. 4(b)). Fig. 5 shows a comparison between *plasmonic* and *standard* miniarrays, for three values of absorption thickness, $1\,\mu m$, $2.5\,\mu m$, and $5\,\mu m$: simulations indicate a reduction of more than one order of magnitude for $\mathcal{D}_{\mathrm{NNs}}$ when t_{abs} is decreased from $5\,\mu m$ to $1\,\mu m$, a very encouraging result, to be extended considering dedicated future investigations along the whole MWIR band. For sake of clarity, it must be remarked that $\mathcal{D}_{\mathrm{NNs}}$ is very similar for *plasmonic* and *standard* miniarrays with the same absorber thickness (it is not expected to be significantly different): actually, the great benefit brought by the adoption of plasmonic detector consists in the possibility to consider much thinner absorber, with performance comparable (e.g., responsivity), better (e.g., detectivity), or much better (e.g., inter-pixel crosstalk) than in standard detectors with thickness in the order of the absorption length.

As a final note, to reach short response times, the absorber thickness should be thin and fully depleted [89]. Let us indicate with $t_{\mathrm{abs,qn}}$ the thickness of the quasi-neutral (or electric field free) region in the absorber, and with $t_{\mathrm{abs,dep}}$ the thickness of its space charge region: the detector response time is governed by the diffusion transit time across the quasi-neutral region, $\tau_{\mathrm{diff}} \approx t_{\mathrm{abs,qn}}^2/D$, and by the drift transit time across the space charge region, $\tau_{\mathrm{drift}} \approx t_{\mathrm{abs,dep}}/(\mu E)$,

where D and μ are, respectively, the minority carrier diffusion coefficient and mobility, and E is the electric field [90, Sec. 4.9]. For both terms, a reduction of the absorber thickness may be beneficial, since it helps reduce both τ_{diff} and τ_{drift}, concurring to decrease the response time.

V. CONCLUSIONS AND PERSPECTIVES

We presented a 3D multiphysics modeling of a planar, HgCdTe-based, diffraction-limited MWIR FPA with $3\,\mu m$ wide pixels and a periodic array of Au nanorods on the illuminated face. Simulations indicate that the proposed plasmonic structure, which employs a $1\,\mu m$-thick absorber layer, exhibits a reduction of diffusive inter-pixel crosstalk by more than one order of magnitude with respect to more conventional, non-plasmonic detectors with $5\,\mu m$-thick absorber, without penalizing responsivity and increasing the detectivity, as well as taking advantage of the absorber volume reduction for what concerns the impact of possible material defects on dark current, paving the way towards a new generation of very thin, subwavelength detectors.

Future work will address simulations of $\mathcal{R}$, D^* and $\mathcal{D}_{\mathrm{NNs}}$ across the whole MWIR band for several doping profiles and operating temperatures, as well as the impact of similar reduced-thickness, plasmonic nanopatterned detectors on the dark current: such an approach may help reduce further cooling requirement, towards the final goal of obtaining satisfactory room-temperature operation. Some details of nanoelement geometry, e.g. the nanorod length t, material(s) and periodicity should be carefully investigated as well, in order to further optimize the light coupling.

REFERENCES

[1] H. Raether, *Surface Plasmons on Smooth and Rough Surfaces and on Gratings*, ser. Springer Tracts in Modern Physics. Berlin: Springer-Verlag, 1988, vol. 111.

[2] Y. Zhong, S. D. Malagari, T. Hamilton, and D. Wasserman, "Review of mid-infrared plasmonic materials," *J. Nanophoton.*, vol. 9, no. 1, p. 093791, 2015.

[3] M. Malerba, A. Alabastri, E. Miele, P. Zilio, M. Patrini, D. Bajoni, G. C. Messina, M. Dipalo, A. Toma, R. P. Zaccaria, and F. D. Angelis, "3D vertical nanostructures for enhanced infrared plasmonics," *Sci. Rep.*, vol. 5, p. 16436, 2015.

[4] P. Biagioni, J.-S. Huang, and B. Hecht, "Nanoantennas for visible and infrared radiation," *Rep. Prog. Phys.*, vol. 75, no. 2, p. 024402, 2012.

[5] J. Rosenberg, R. V. Shenoi, S. Krishna, and O. Painter, "Design of plasmonic photonic crystal resonant cavities for polarization sensitive infrared photodetectors," *Opt. Express*, vol. 18, no. 4, pp. 3672–3686, 2010.

[6] S. Q. Li, P. Guo, L. Zhang, W. Zhou, T. W. Odom, T. Seideman, J. B. Ketterson, and R. P. H. Chang, "Infrared plasmonics with indium-tin-oxide nanorod arrays," *ACS Nano*, vol. 5, no. 11, pp. 9161–9170, 2011.

[7] A. Agrawal, I. Kriegel, and D. J. Milliron, "Shape-dependent field enhancement and plasmon resonance of oxide nanocrystals," *J. Phys. Chem. C*, vol. 119, no. 11, pp. 6227–6238, 2011.

[8] J. Tong, L. Y. M. Tobing, S. Qiu, D. H. Zhang, and A. G. U. Perera, "Room temperature plasmon-enhanced InAs$_{0.91}$Sb$_{0.09}$-based heterojunction *n-i-p* mid-wave infrared photodetector," *Appl. Phys. Lett.*, vol. 113, no. 1, p. 011110, 2018.

[9] K. Tappura, "Enhancing the performance of commercial infrared detectors by surface plasmons," *MDPI Proc.*, vol. 2, no. 13, p. 1063, 2018.

[10] N. Vanamala, K. C. Santiago, and N. C. Das, "Enhanced MWIR absorption of HgCdTe (MCT) via plasmonic metal oxide nanostructures," *AIP Adv.*, vol. 9, p. 025113, 2019.

[11] N. Vanamala, K. C. Santiago, N. C. Das, and S. K. Hargrove, "Geometric optimization of plasmonic nanostructure arrays on MWIR HgCdTe (MCT)," *AIP Adv.*, vol. 10, p. 065006, 2020.

[12] J. Budhu, N. Pfiester, K.-K. Choi, S. Young, C. Ball, S. Krishna, and A. Grbic, "Dielectric resonator antenna coupled antimonide-based detectors (DRACAD) for the infrared," *IEEE Trans. Antennas Propagation*, 2021.

[13] J. Liang, W. D. Hu, X. S. Chen, Z. F. Li, and W. Lu, "Modeling of HgCdTe photoconductive infrared detector with metallic nanostructures," in *20th International Conference on Numerical Simulation of Optoelectronic Devices (NUSOD 2020)*, Palma de Mallorca, Spain, Sept. 2014, pp. 179–180.

[14] A. Rogalski, *Infrared Detectors*, 2nd ed. Boca Raton, FL: CRC Press, 2011.

[15] K. D. Smith, J. G. A. Wehner, R. W. Graham, J. E. Randolph, A. M. Ramirez, G. M. Venzor, K. Olsson, M. F. Vilela, and E. P. G. Smith, "High operating temperature mid-wavelength infrared HgCdTe photon trapping focal plane arrays," in *Infrared Technology and Applications XXXVIII*, vol. 8353, Proceedings of the SPIE. SPIE, 2012, pp. 972–978.

[16] Y. U. Jung, I. Bendoym, and D. T. Crouse, "Numerical study of near-, mid-, and long-infrared photon trapping in crystalline and amorphous HgCdTe metamaterials," *Appl. Phys. A*, vol. 122, no. 4, p. 376, 2016.

[17] T. Ashley and C. T. Elliott, "Model for minority carrier lifetimes in doped HgCdTe," *Electron. Lett.*, vol. 21, no. 10, pp. 451–452, 1985.

[18] C. T. Elliott, "Non-equilibrium modes of operation of narrow-gap semiconductor devices," *Semiconductor Sci. Technol.*, vol. 5, no. 35, p. S30, 1990.

[19] B. Debbrecht, M. McElhiney, V. Carey, C. Cullen, M. S. Mirotznik, and B. G. DeLacy, "Cavity-based aluminum nanohole arrays with tunable infrared resonances," *Opt. Express*, vol. 25, no. 20, pp. 24 501–24 511, 2017.

[20] K. Nakayama, K. Tanabe, and H. A. Atwater, "Plasmonic nanoparticle enhanced light absorption in GaAs solar cells," *Appl. Phys. Lett.*, vol. 93, no. 12, p. 121904, 2008.

[21] H. Yu, Y. Peng, Y. Yang, and Z.-Y.Li, "Plasmon-enhanced light–matter interactions and applications," *npj Comput. Mater.*, vol. 5, no. 1, p. 45, 2018.

[22] G. Singh and S. S. Verma, "Plasmonic periodic nanostructures for enhanced photovoltaic response in thin film GaAs solar cells," *Opt. Eng.*, vol. 59, no. 12, pp. 1–15, 2020.

[23] S. C. Lee, S. Krishna, and S. R. J. Brueck, "Light direction-dependent plasmonic enhancement in quantum dot infrared photodetectors," *Appl. Phys. Lett.*, vol. 97, no. 2, p. 021112, 2010.

[24] G. Gu, N. Mojaverian, J. Vaillancourt, and X. Lu, "Surface plasmonic resonance induced near-field vectors and their contribution to quantum dot infrared photodetector enhancement," *J. Phys. D*, vol. 47, no. 43, p. 435106, 2014.

[25] J. Y. Andersson and L. Lundqvist, "Near-unity quantum efficiency of AlGaAs/GaAs quantum well infrared detectors using a waveguide with a doubly periodic grating coupler," *Appl. Phys. Lett.*, vol. 59, no. 7, pp. 857–859, 1991.

[26] M. Zamiri, E. Plis, J. O. Kim, S. C. Lee, A. Neumann, S. Myers, E. P. Smith, A. M. Itsuno, J. G. A. Wehner, S. M. Johnson, S. R. J. Brueck, and S. Krishna, "MWIR superlattice detectors integrated with substrate side-illuminated plasmonic coupler," in *Infrared Technology and Applications XL*, vol. 9070, Proceedings of the SPIE. SPIE, 2014, p. 90700Y.

[27] K. K. Choi, M. D. Jhabvala, J. Sun, C. A. Jhabvala, A. Waczynski, and K. Olvera, "Resonator-QWIPs and FPAs," in *Infrared Technology and Applications XL*, vol. 9070, Proceedings of the SPIE. SPIE, 2014, p. 907037.

[28] E. M. Jackson, J. A. Nolde, M. Kim, C. S. Kim, E. R. Cleveland, C. A. Affouda, C. L. Canedy, I. Vurgaftman, J. R. Meyer, E. H. Aifer, and J. Lorentzen, "Two-dimensional plasmonic grating for increased quantum efficiency in midwave infrared nBn detectors with thin absorbers," *Opt. Express*, vol. 26, no. 11, pp. 13 850–13 864, 2018.

[29] S. Maimon and G. W. Wicks, "*nBn* detector, an infrared detector with reduced dark current and higher operating temperature," *Appl. Phys. Lett.*, vol. 89, no. 15, p. 151109, 2006.

[30] J. Li, J.-Z. Li, H. Zhou, G. Zhang, H. Liu, S.-W. Wang, and F. Yi, "Plasmonic metamaterial absorbers upon strong coupling effects for small pixel infrared detector," *Opt. Express*, vol. 29, no. 15, pp. 22 907–22 921, 2021.

[31] H. Ge, R. Xie, Y. Chen, P. Wang, Q. Li, Y. Gu, J. Guo, J. He, F. Wang, and W. Hu, "Skin effect photon-trapping enhancement in infrared photodiodes," *Opt. Express*, vol. 29, no. 15, pp. 22 823–22 837, 2021.

[32] P. Martyniuk, J. Antoszewski, M. Martyniuk, L. Faraone, and A. Rogalski, "New concepts in infrared photodetector designs," *Appl. Phys. Rev.*, vol. 1, p. 041102, 2014.

[33] R. K. Bhan and V. Dhar, "Recent infrared detector technologies, applications, trends and development of HgCdTe based cooled infrared focal plane arrays and their characterization," *Opto-Electron. Rev.*, vol. 27, no. 2, pp. 174–193, 2019.

[34] M. Vallone, M. Goano, F. Bertazzi, G. Ghione, S. Hanna, D. Eich, A. Sieck, and H. Figgemeier, "Constraints and performance tradeoffs in Auger-suppressed HgCdTe focal plane arrays," *Appl. Opt.*, vol. 59, no. 17, pp. E1–E8, June 2020.

[35] M. Vallone, M. Goano, A. Tibaldi, S. Hanna, D. Eich, A. Sieck, H. Figgemeier, G. Ghione, and F. Bertazzi, "Challenges in multiphysics modeling of dual-band HgCdTe infrared detectors," *Appl. Opt.*, vol. 59, no. 19, pp. 5656–5663, July 2020.

[36] M. A. Kinch, "The future of infrared; III-Vs or HgCdTe?" *J. Electron. Mater.*, vol. 44, no. 9, pp. 2969–2976, 2015.

[37] M. Vallone, M. Mandurrino, M. Goano, F. Bertazzi, G. Ghione, W. Schirmacher, S. Hanna, and H. Figgemeier, "Numerical modeling of SRH and tunneling mechanisms in high-operating-temperature MWIR HgCdTe photodetectors," *J. Electron. Mater.*, vol. 44, no. 9, pp. 3056–3063, 2015.

[38] D. Eich, W. Schirmacher, and S. Hanna, "Progress of MCT detector technology at AIM towards smaller pitch and lower dark current," *J. Electron. Mater.*, vol. 46, no. 9, pp. 5448–5457, 2017.

[39] H. A. Macleod, *Thin film optical filters, 4th Ed.*, E. R. Pike and R. G. W. Brown, Eds. New York, USA: CRC Press, 2010.

[40] D. Lee, M. Carmody, E. Piquette, P. Dreiske, A. Chen, A. Yulius, D. Edwall, S. Bhargava, M. Zandian, and W. Tennant, "High-operating temperature HgCdTe: A vision for the near future," *J. Electron. Mater.*, vol. 45, no. 9, pp. 4587–4595, 2016.

[41] C. L. Tan and H. Mohseni, "Emerging technologies for high performance infrared detectors," *Nanophoton.*, vol. 7, no. 1, pp. 169–197, 2018.

[42] D. S. Hobbs and B. D. MacLeod, "Design, fabrication, and measured performance of anti-reflecting surface textures in infrared transmitting materials," in *Window and dome technologies and materials IX*, vol. 5786, Proceedings of the SPIE. SPIE, 2005, pp. 349–364.

[43] B. D. MacLeod and D. S. Hobbs, "Long life, high performance anti-reflection treatment for HgCdTe infrared focal plane arrays," in *Infrared Technology and Applications XXXIV*, vol. 6940, Proceedings of the SPIE. SPIE, 2008, p. 69400Y.

[44] J. Schuster, B. Pinkie, S. Tobin, C. Keasler, D. D'Orsogna, and E. Bellotti, "Numerical simulation of third-generation HgCdTe detector pixel arrays," *IEEE J. Select. Topics Quantum Electron.*, vol. 19, no. 5, p. 800415, 2013.

[45] A. Rogalski, P. Martyniuk, and M. Kopytko, "Challenges of small-pixel infrared detectors: a review," *Rep. Prog. Phys.*, vol. 79, no. 4, p. 046501, 2016.

[46] L. Macé, E. H. Oubensaid, F. Pradal, R. Lhuillier, H. Leplan, O. Gauthier-Lafaye, and A. Monmayrant, "Progress in thin film coating on space IR detectors," in *International Conference on Space Optics – ICSO 2018*, vol. 11180, Proceedings of the SPIE. SPIE, 2019, pp. 1310–1318.

[47] R. Orta, A. Tibaldi, and P. Debernardi, "Bimodal resonance phenomena–part II: high/low-contrast grating resonators," *IEEE J. Quantum Electron.*, vol. 52, no. 12, pp. 6 600 409–1–8, 2016.

[48] Y. F. Huang and S. Chattopadhyay, "Nanostructure surface design for broadband and angle-independent antireflection," *J. Nanophoton.*, vol. 7, no. 1, pp. 1–10, 2013.

[49] M. A. Kinch, "Fundamental physics of infrared detector materials," *J. Electron. Mater.*, vol. 29, no. 6, pp. 809–817, 2000.

[50] J. Schuster, R. E. DeWames, and P. S. Wijewarnasurya, "Dark currents in a fully-depleted LWIR HgCdTe *P*-on-*n* heterojunction: analytical and numerical simulations," *J. Electron. Mater.*, vol. 46, no. 11, pp. 6295–6305, 2017.

[51] G. C. Holst and R. G. Driggers, "Small detectors in infrared system design," *Opt. Eng.*, vol. 51, no. 9, p. 096401, 2012.

[52] B. Pinkie and E. Bellotti, "Numerical simulation of spatial and spectral crosstalk in two-color MWIR/LWIR HgCdTe infrared detector arrays," *J. Electron. Mater.*, vol. 42, no. 11, pp. 3080–3089, 2013.

[53] M. Vallone, M. Goano, F. Bertazzi, G. Ghione, S. Hanna, D. Eich, and H. Figgemeier, "Diffusive-probabilistic model for inter-pixel crosstalk in HgCdTe focal plane arrays," *IEEE J. Electron Devices Soc.*, vol. 6, no. 1, pp. 664–673, 2018.

[54] M. Vallone, M. Goano, F. Bertazzi, G. Ghione, A. Palmieri, S. Hanna, D. Eich, and H. Figgemeier, "Reducing inter-pixel crosstalk in HgCdTe detectors," *Opt. Quantum Electron.*, vol. 52, no. 1, p. 25, 2020.

[55] C. A. Hougen, "Model for infrared absorption and transmission of liquid-phase epitaxy $Hg_{1-x}Cd_xTe$," *J. Appl. Phys.*, vol. 66, no. 8, pp. 3763–3766, 1989.

[56] M. A. Ordal, L. L. Long, R. J. Bell, S. E. Bell, R. R. Bell, R. W. Alexander, and C. A. Ward, "Optical properties of the metals Al, Co, Cu, Au, Fe, Pb, Ni, Pd, Pt, Ag, Ti, and W in the infrared and far infrared," *Appl. Opt.*, vol. 22, no. 7, pp. 1099–1119, 1983.

[57] G. D. Boreman, *Modulation Transfer Function in Optical and Electro-Optical Systems.* Bellingham, WA: SPIE, 2001.

[58] R. G. Driggers, R. Vollmerhausen, J. P. Reynolds, J. Fanning, and G. C. Holst, "Infrared detector size: how low should you go?" *Opt. Eng.*, vol. 51, no. 6, p. 063202, 2012.

[59] G. C. Holst, R. Driggers, and O. Furxhi, "Design considerations for advanced MWIR target acquisition systems," *Appl. Opt.*, vol. 59, no. 14, pp. 4339–4348, 2020.

[60] Z. Fan, D. J. Ruebusch, A. A. Rathore, R. Kapadia, O. Ergen, P. W. Leu, and A. Javey, "Challenges and prospects of nanopillar-based solar cells," *Nano Res.*, vol. 2, pp. 829–843, 2009.

[61] J. Liu, S. Zhang, Y. Ma, J. Shao, B. Lu, and Y. Chen, "Gold nanopillar arrays as biosensors fabricated by electron beam lithography combined with electroplating," *Appl. Opt.*, vol. 54, no. 9, pp. 2537–2542, 2015.

[62] S.-J. Tsai, M. Ballarotto, D. B. Romero, W. N. Herman, H.-C. Kan, and R. J. Phaneuf, "Effect of gold nanopillar arrays on the absorption spectrum of a bulk heterojunction organic solar cell," *Opt. Express*, vol. 18, no. s4, pp. A528–A535, 2010.

[63] K. Yu, A. Lakhani, and M. C. Wu, "Subwavelength metal-optic semiconductor nanopatch lasers," *Opt. Express*, vol. 18, no. 9, pp. 8790–8799, 2010.

[64] C.-C. Chang, Y. D. Sharma, Y.-S. Kim, J. A. Bur, R. V. Shenoi, S. Krishna, D. Huang, and S.-Y. Lin, "A surface plasmon enhanced infrared photodetector based on InAs quantum dots," *Nano Lett.*, vol. 10, no. 5, pp. 1704–1709, 2010.

[65] A. Karar, N. Das, C. L. Tan, K. Alameh, Y. T. Lee, and F. Karouta, "High-responsivity plasmonics-based GaAs metal-semiconductor-metal photodetectors," *Appl. Phys. Lett.*, vol. 99, no. 13, p. 133112, 2010.

[66] J.-P. Berenger, "A perfectly matched layer for the absorption of electromagnetic waves," *J. Comp. Phys.*, vol. 114, no. 2, pp. 185–200, 1994.

[67] M. Vallone, M. Goano, F. Bertazzi, G. Ghione, S. Hanna, D. Eich, and H. Figgemeier, "FDTD simulation of compositionally graded HgCdTe photodetectors," *Infrared Phys. Technol.*, vol. 97, pp. 203–209, 2019.

[68] *RSoft FullWAVE User Guide, v2017.03*, Synopsys, Inc., Inc., Optical Solutions Group, Ossining, NY, 2017.

[69] J. D. Jackson, *Classical Electrodynamics*, 3rd ed. New York, USA: Wiley, 1999.

[70] M. Born and E. Wolf, *Principles of Optics. Electromagnetic Theory of Propagation, Interference and Diffraction of Light*, 7th ed. Cambridge, U.K.: Cambridge University Press, 1999.

[71] S. J. Orfanidis, "Electromagnetic waves and antennas," https://www.ece.rutgers.edu/ orfanidi/ewa/, 2016. [Online]. Available: https://www.ece.rutgers.edu/~orfanidi/ewa/

[72] C. Keasler and E. Bellotti, "Three-dimensional electromagnetic and electrical simulation of HgCdTe pixel arrays," *J. Electron. Mater.*, vol. 40, no. 8, pp. 1795–1801, 2011.

[73] J. Liang, W. Hu, Z. Ye, L. Liao, Z. Li, X. Chen, and W. Lu, "Improved performance of HgCdTe infrared detector focal plane arrays by modulating light field based on photonic crystal structure," *J. Appl. Phys.*, vol. 115, no. 18, p. 184504, 2014.

[74] O. Akın and H.-V. Demir, "High-efficiency low-crosstalk dielectric metasurfaces of mid-wave infrared focal plane arrays," *Appl. Phys. Lett.*, vol. 110, p. 143106, 2017.

[75] M. Vallone, M. Goano, F. Bertazzi, G. Ghione, W. Schirmacher, S. Hanna, and H. Figgemeier, "Comparing FDTD and ray tracing models in the numerical simulation of HgCdTe LWIR photodetectors," *J. Electron. Mater.*, vol. 45, no. 9, pp. 4524–4531, 2016.

[76] ——, "Simulation of small-pitch HgCdTe photodetectors," *J. Electron. Mater.*, vol. 46, no. 9, pp. 5458–5470, 2017.

[77] A. Tibaldi, M. Ghomashi, F. Bertazzi, M. Goano, M. Vallone, and G. Ghione, "Plasmonic-organic hybrid electro/optic Mach-Zehnder modulators: from waveguide to multiphysics modal-FDTD modeling," *Opt. Express*, vol. 28, no. 20, pp. 29 253–29 271, Sept. 2020.

[78] M. Vallone, M. Goano, A. Tibaldi, S. Hanna, A. Wegmann, D. Eich, H. Figgemeier, G. Ghione, and F. Bertazzi, "Quantum efficiency and crosstalk in subwavelength HgCdTe dual band infrared detectors," *IEEE J. Select. Topics Quantum Electron.*, vol. 28, no. 2, p. 3800309, Mar./Apr. 2022.

[79] *Sentaurus Device User Guide. Version N-2017.09*, Synopsys, Inc., Mountain View, CA, Sept. 2017.

[80] V. Nathan, "Optical absorption in $Hg_{1-x}Cd_xTe$," *J. Appl. Phys.*, vol. 83, no. 5, pp. 2812–2814, 1998.

[81] J. Chu and A. Sher, *Physics and Properties of Narrow Gap Semiconductors.* New York: Springer-Verlag, 2008.

[82] V. C. Lopes, A. J. Syllaios, and M. C. Chen, "Minority carrier lifetime in mercury cadmium telluride," *Semiconductor Sci. Technol.*, vol. 8, no. 6S, pp. 824–841, June 1993.

[83] M. Mandurrino, G. Verzellesi, M. Goano, M. Vallone, F. Bertazzi, G. Ghione, M. Meneghini, G. Meneghesso, and E. Zanoni, "Trap-assisted tunneling in InGaN/GaN LEDs: experiments and physics-based simulation," in *14th International Conference on Numerical Simulation of Optoelectronic Devices (NUSOD 2014)*, Palma de Mallorca, Spain, Sept. 2014, pp. 13–14.

[84] M. Mandurrino, M. Goano, M. Vallone, F. Bertazzi, G. Ghione, G. Verzellesi, M. Meneghini, G. Meneghesso, and E. Zanoni, "Semiclassical simulation of trap-assisted tunneling in GaN-based light-emitting diodes," *J. Comp. Electron.*, vol. 14, no. 2, pp. 444–455, June 2015.

[85] M. Mandurrino, G. Verzellesi, M. Goano, M. Vallone, F. Bertazzi, G. Ghione, M. Meneghini, G. Meneghesso, and E. Zanoni, "Physics-based modeling and experimental implications of trap-assisted tunneling in InGaN/GaN light-emitting diodes," *Phys. Status Solidi A*, vol. 212, no. 5, pp. 947–953, 2015.

[86] J. Rosenberg, R. V. Shenoi, S. Krishna, and O. Painter, "Evaluation of HgCdTe on GaAs grown by molecular beam epitaxy for high-operating-temperature infrared detector applications," *J. Electron. Mater.*, vol. 44, no. 9, pp. 3002–3006, 2015.

[87] M. A. Kinch, *State-of-the-Art Infrared Detector Technology.* Bellingham, WA: SPIE, 2014.

[88] B. K. Shukla and R. H. Patel, "Simulation of paraxial beam propagation using plane wave expansion method," in *2008 International conference on recent advances in microwave theory and applications.* IEEE, 2008, pp. 652–656.

[89] A. Rogalski, P. Martyniuk, M. Kopytko, and W. Hu, "Trends in performance limits of the HOT infrared photodetectors," *MDPI Appl. Sci.*, vol. 11, no. 2, p. 501, 2021.

[90] G. Ghione, *Semiconductor Devices for High-Speed Optoelectronics.* Cambridge, U.K.: Cambridge University Press, 2009.

Marco Vallone received the M.Sc in Physics from the Università di Torino (Italy) and Ph.D. in Electronic Devices by the Politecnico di Torino (Italy) in 1985 and 2016 respectively. During 1985 - 2008 he was first with Telecom Italia, then with Avago Technologies, working on testing and modeling of optoelectronic devices. Since 2008 he holds a Post-Doctoral position at the Politecnico di Torino, where he is currently assistant professor. His current research activity is focused on the simulation of optoelectronic devices based on narrow- and wide-bandgap semiconductor materials, and on the description of inter- and intra-band quantum scattering processes.

Alberto Tibaldi (M'19) received the B.Sc., M.Sc., and Ph.D. degrees in electronic engineering from the Polytechnic of Turin, in 2009, 2011 and 2015, respectively. From 2012 to 2019, he was with the Italian National Council of Research (CNR) as a Research Fellow. Since 2019, he has been with the Department of Electronics and Telecommunications, Polytechnic of Turin as an Assistant Professor, where he teaches courses on semiconductor devices and numerical analysis. His scientific interests mainly regard the multi-physics modeling of optoelectronic devices.

Stefan Hanna received the M.Sc. degree in physics and the Ph.D. degree from Universität Bayreuth, Germany, in 2002 and 2008, respectively. He has been with AIM Infrarot-Module GmbH since 2007, working from 2007 to 2010 in the electro-optical characterization of SWIR, LWIR, and VLWIR detectors for space applications within the space projects group of the AIM Division Sensors. From 2008 to 2015, he was a Project Manager of various TRP research and development studies with the European Space Agency, and with the System Design of the AIM Division Space Program from 2014 to 2017, he was working in sensor development within the AIM Division Sensors. Since 2018, he is a Manager with Photodiode Array Development, Division Sensors, AIM.

Anne Wegmann received the M.Sc. degree in physics from Universität Münster, Germany, in 2010 and the Ph.D. degree from Universität Heidelberg, Germany, in 2017. She has been with AIM Infrarot-Module GmbH since 2018, working from 2018 to 2019 in the electro-optical characterization of SWIR, LWIR, and VLWIR detectors for space applications within the space projects group of the AIM Division Sensors. From 2018 to 2020 she was a technical manager of a TRP program with the European Space Agency. Since 2020, she has been working in the sensor development group within the AIM Division Sensors.

Detlef Eich received the M.Sc. degree in physics and the Ph.D. degree from Universität Würzburg, Germany, in 1996 and 2000, respectively. He has been with AIM Infrarot-Module GmbH, Heilbronn, since 2000. From 2000 to 2009, he was a Development Staff Member with the Development of FPA Technology for CMT IR Photodetectors, Division Sensors, AIM. From 2009 to 2012, he was a Manager with the Development FPA-Technology, Division Sensors. From 2012 to 2014, he was a Manager with Operations Projects, Division Sensors. Since 2014, he has been a Manager with Development, Division Sensors.

Heinrich Figgemeier received the M.Sc. degree in physics from Universität Paderborn, Germany, in 1989. From 1989 to 1995, he was with AEG, Heilbronn, as a Development Staff Member with the Development of Liquid Phase Epitaxy for CMT IR Photodetectors. In 1996, he joined AIM Infrarot-Module GmbH, where he is a Manager of Product Planning and FPA-Technology, Division Sensors from 1996 to 2009. From 2009 to 2013, he was a Manager with Division Sensors, AIM, and since 2014, he is the Head of Division Sensors, AIM.

Giovanni Ghione graduated (cum laude) in electronic engineering from the Politecnico di Torino, in 1981. Since 1990, he has been a Full Professor in electronics, from 1991 again with the Politecnico di Torino. He has authored or coauthored more than 350 research articles on the above subjects and four books. His research activity has mainly concerned the high-frequency electronics, with particular attention to the physics-based modeling of compound semiconductor materials and devices and to the design of microwave ICs. He is also involved in research on optoelectronic devices, with application to high-speed photodetector and to electro-optic and electro-absorption modulator modeling, more recently within the framework of Si photonics, but also to FIR detectors and to organic and nanodot solar cells. He is a reviewer for several international journals and a member of the Editorial Board of the MTT Transactions. He was the EU Arrangement Chair of IEDM, from 2009 to 2010. He also chaired the ED Society Committee on Compound Semiconductor Devices and Circuits, from 2010 to 2015. From 2010 to 2015, he has been an Associate Editor of the IEEE T-ED. He is the T-ED Editor in Chief (2016–2021)

Francesco Bertazzi received the Laurea and Ph.D. degrees in electronics engineering from the Politecnico di Torino, Turin, Italy, in 2000 and 2003, respectively. He was a Visiting Scholar with the Department of Electrical and Computer Engineering at Boston University, Boston, MA. Since 2008 he is professor at the Dipartimento di Elettronica, Politecnico di Torino. His PhD studies were focused on electromagnetic modeling of traveling-wave structures for optoelectronic applications and nonlinear physics-based noise analysis of RF and microwave devices. His research activities at Boston University included material-theory-based modeling of band structures, vibrational properties, and carrier scattering rates, essential for the study of the complex electronic, transport, and optical properties of novel wide-gap semiconductors, in particular III-nitrides and II-VI oxide semiconductors. His present research activity is focused on density matrix and nonequilibrium Green's function modeling of carrier transport and recombination processes in optoelectronic devices (HgCdTe infrared photodetectors, InGaN light-emitting diodes and VCSELs).

Michele Goano (M'98, SM'19) received the Laurea and Ph.D. degrees in electronic engineering from Politecnico di Torino, Turin, Italy, in 1989 and 1993, respectively. In 1994 and 1994, he was a Post-Doctoral Fellow with the Département de Génie Physique, École Polytechnique de Montréal, Montréal, QC, Canada. He joined the faculty of Politecnico di Torino in 1995. He has been a visiting scholar with the School of Electrical and Computer Engineering, Georgia Institute of Technology, Atlanta, GA, USA, with the Department of Information Technology and Media, Mid-Sweden University, Sundsvall, Sweden, and with the Department of Electrical and Computer Engineering, Boston University, Boston, MA, USA. His current research activity is focused on the simulation of optoelectronic devices based on narrow- and wide-bandgap semiconductor materials.